catalysts

MDPI

Article

Electrochemical Removal of NO_x on Ceria-Based Catalyst-Electrodes

Xi Wang [1,2], Alexandre Westermann [1], Yi Xiang Shi [2], Ning Sheng Cai [2], Mathilde Rieu [3], Jean-Paul Viricelle [3] and Philippe Vernoux [1,*]

1 Université de Lyon, CNRS, Université Claude Bernard Lyon 1, IRCELYON, UMR 5256, 2 Avenue A. Einstein, 69626 Villeurbanne, France; w-q12@mails.tsinghua.edu.cn (X.W.); alexandre.westermann@ircelyon.univ-lyon1.fr (A.W.)

2 Key Laboratory for Thermal Science and Power Engineering of Ministry of Education, Tsinghua University, 100084 Beijing, China; shyx@mail.tsinghua.edu.cn (Y.X.S.); cains@tsinghua.edu.cn (N.S.C.)

3 Ecole Nationale Supérieure des Mines, SPIN-EMSE, CNRS: UMR5307, LGF, F-42023 Saint-Etienne, France; rieu@emse.fr (M.R.); viricelle@emse.fr (J.-P.V.)

* Correspondence: philippe.vernoux@ircelyon.univ-lyon1.fr; Tel.:+33-4-7243-1587

Academic Editors: Enrique Rodríguez-Castellón, Agustín Bueno-López and Elisa Moretti
Received: 23 December 2016; Accepted: 8 February 2017; Published: 16 February 2017

Abstract: This study reports the electrochemical properties for NO_x reduction of a ceria-based mixed ionic electronic conducting porous electrode promoted by Pt nanoparticles, as efficient catalyst for NO oxidation, and BaO, as sorbent to store NO_x. This catalytic layer was deposited by screen-printing on a dense membrane of gadolinia-doped ceria, an O^{2-} ionic conductor. The targeted Ba and Pt loadings were 150 and 5 $\mu g/cm^2$, respectively. The NO_x selective electrochemical reduction was performed between 400 °C and 500 °C with and without oxygen in the feed. Variations of the open-circuit voltage with time were found to be a good sensor of the NO_x storage process on the ceria-based catalyst-electrode. However, no N_2 production was observed in the presence of O_2 phase in spite of nitrates formation.

Keywords: nitrogen oxides; gadolinia-doped ceria; BaO; Pt; NO_x storage; NO_x electrochemical reduction

1. Introduction

Nitrogen oxides (NO_x: NO + NO_2) are pollutants mainly emitted by thermal engines using fossil fuels. They are at the origin of safety problems. The design of more efficient and stable catalysts to reduce NO_x to nitrogen in atmospheres containing an excess of oxygen, such as exhaust gas emitted by diesel and lean-burn gasoline engines, has attracted much attention in the last years. Due to the more and more stringent emission standards, an efficient and clean technology to control the NO_x emissions from automotive engines becomes an important demand. In Europe [1], the NO_x emission limit is 80 mg/km for diesel passenger cars according to the Euro 6 standard in force since 2014. The two actual technologies on the market are using an additional reducing agent to remove NO_x, i.e., diesel fuel post-injections for the NO_x Lean Trap Catalyst (LTC) and urea for the Selective Catalytic Reduction (SCR) [2]. The former is containing Pt and BaO for the oxidation NO into NO_2, and the storage of NO_2 as nitrates, respectively. When the LTC surface is saturated by nitrates, a diesel post injection is triggered for few seconds to decompose nitrates and reduce NO_x into N_2. However, these periodic short rich phases provoke a fuel overconsumption. SCR catalysts are based on zeolite materials which are cheap and robust but the control of the urea injection to avoid NH_3 release is tricky. In addition, recent studies on the on-road emissions of NO_x from Euro 6 Diesel vehicles have clearly shown that these two technologies are not sufficiently effective to comply the standards. Therefore, alternative solutions have to be developed. One promising solution could be the Selective Electrochemical Reduction (SER)

of NO_x into N_2 in a Solid Oxide Electrolysis Cell (SOEC). This latter process does not need an additional reducing agent to reduce NO_x. The reduction is ensured by a cathodic polarization. Then, SER saves the large reducing agent storage system and avoids the emission of pollutants such as NH_3 (SCR) or VOC (LTC) produced by the reducing agents [3–5]. It was first proposed by Pancharatnam et al. [6] in 1976 that NO can be electrochemically reduced into N_2 on a Pt cathode interfaced on an oxygen ionic conductor. The reaction mechanism was investigated by Gür and Huggins [7] in 1979. However, diesel exhausts contain a large quantity of oxygen. The competitive electrochemical reduction of O_2 into O^{2-} is much faster than the SER of NO_x on a Pt electrode [8]. To improve the selectivity of the NO_x electrochemical conversion, some researchers have recently shown that the addition of a NO_x sorbent (K, Ba) can promote SER of NO_x into N_2 [9–12]. Two approaches are proposed in the literature. The former deals with multilayers configurations with a NO_x adsorption layer deposited at the top of a catalyst-electrode layer [9,11]. The latter seems to be more promising and refers to the infiltration of a NO_x sorbent, such as BaO, into the porosity of the catalyst-electrode [12–14]. For instance, remarkable results have been obtained with the infiltration of both BaO particles and a Pt/Al_2O_3 catalyst into the porosity of symmetrical electrodes of $(La_{0.85}Sr_{0.15})_{0.99}MnO_3$ (LSM) interfaced on a dense GDC membrane [12]. At 450 °C, NO_x conversion and N_2 selectivity as high as 65% and 86%, respectively, were achieved in an excess of oxygen.

The objective of this study was to infiltrate both BaO and Pt nanoparticles in the porosity of a ceria-based electrode layer to delocalize the SER of NO_x into the whole volume of the electrode. The mixed ionic electronic conducting (MIEC) coating was a composite electrode between LSCF ($La_{0.6}Sr_{0.4}Co_{0.8}Fe_{0.2}O_{3-\delta}$) and GDC ($Gd_{0.2}Ce_{0.8}O_{1.9}$), able to conduct both O^{2-} and electrons. A dense membrane of GDC was used as the electrolyte due to its high ionic conductivity at low temperature [15,16]. The NO_x electrocatalytic performances were investigated between 400 °C and 500 °C in $NO/O_2/He$ atmospheres.

2. Results and Discussion

2.1. Catalyst-Electrode Characterizations

The Pt-BaO/LSCF-GDC electrode structure and morphology were characterized by SEM (Scanning Electronic Microscopy). The thickness of the LSCF/GDC electrode was around 10 µm (Figure 1a). The morphology of the LSFC-GDC composite layer was shown on Figure 1b. The electrode is made of micrometric and agglomerated grains, probably due to the high calcination temperature used during the preparation (1200 °C). Pores size is around 1–3 µm. TEM (Transmission Electronic Microscopy) observations after the extractive replica preparation method of the samples, have revealed the presence of Pt nanoparticles. Figure 2 shows a typical Pt nanoparticle. The mean diameter of Pt nanoparticles was around 10 nm. Unfortunately, BaO particles were not detected neither with SEM, most probably due to small grain sizes, nor with TEM. This suggests that BaO particles are heterogeneously distributed in the electrode. Recently, the group of K. Kammer Hansen [3] has infiltrated BaO in the porosity of a similar cell made of 60 wt % of $La_{0.85}Sr_{0.15}Co_xMn_{1-x}O_{3+\delta}$ and 40 wt % of $Ce_{0.9}Gd_{0.1}O_{1.95}$. They have shown that BaO nanoparticles in the inner layers are only present on the LSM phase. Therefore, BaO in our case, could be preferentially localized on LSCF grains.

2.2. NO_x Electrocatalytic Conversions without Oxygen in the Feed

The parameter ΔNO_x difference between inlet ($NO_{x,in}$) and outlet ($NO_{x,out}$) concentrations of NO_x ($NO + NO_2$), was used to highlight the NO_x storage process as nitrates on the catalyst-electrode. Upon open-circuit voltage (OCV), without any polarization and then electrochemical reaction, positive values of ΔNO_x indicate that a part of NO_x species is stored on the catalyst-electrode.

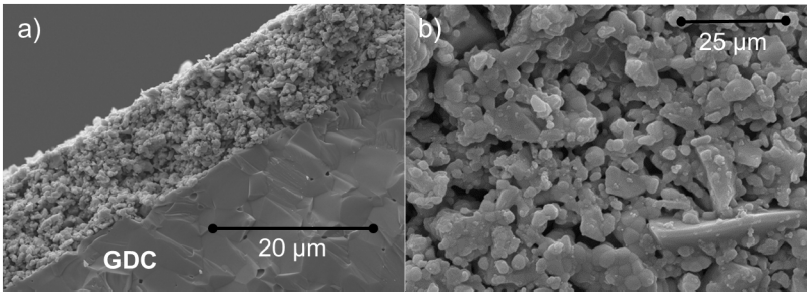

Figure 1. (**a**) Cross section SEM (Scanning Electronic Microscopy) image of the Pt-BaO/LSCF ($La_{0.6}Sr_{0.4}Co_{0.8}Fe_{0.2}O_{3-\delta}$)-GDC ($Gd_{0.2}Ce_{0.8}O_{1.9}$)/GDC cell and (**b**) SEM image of the surface of the catalyst-electrode.

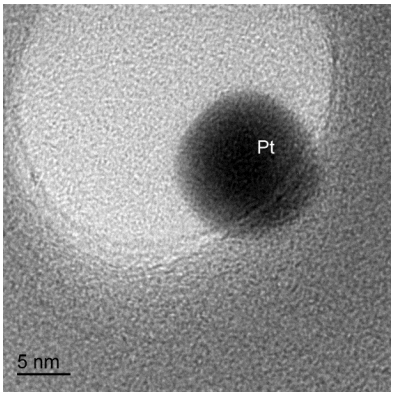

Figure 2. TEM ((Transmission Electronic Microscopy) image of a Pt nanoparticle infiltrated in the catalyst-electrode.

Figure 3 shows variations of OCV (Open-Circuit Voltage) and ΔNO_x with time at 500 °C. Initial positive values of ΔNO_x confirm that a part of NO_x is stored on the catalyst-electrode, most probably on BaO sites as $Ba(NO_3)_2$. Similar experiments carried out with a Ba free composite electrode gave negligible values of ΔNO_x, then confirming the active role of BaO to store NO_x.

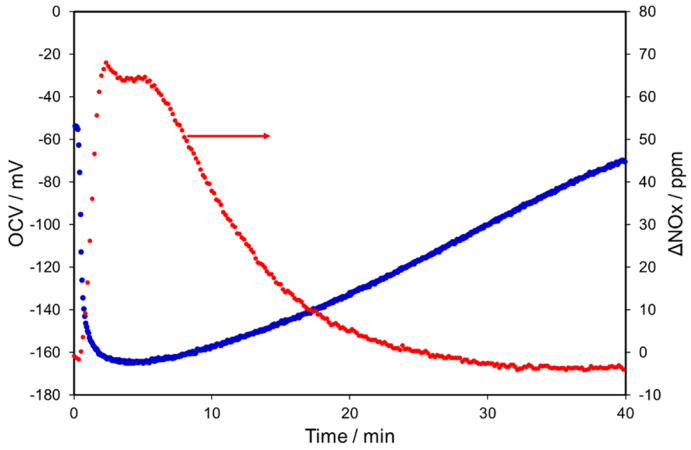

Figure 3. Variations of open-circuit voltage (OCV) and ΔNO_x as a function of time at 500 °C. Reactive mixture: NO/NO_2: 680 ppm/10 ppm in He.

On the complete composite electrode, traces of oxygen in the feed or oxygens stored in GDC allow the catalytic production of NO_2 on Pt nanoparticles. An NO_2 production peak at around 40 ppm was

detected 4 min after the reactants introduction, corresponding to the beginning of the ΔNO_x plateau. The duration of this latter is approximately 3 min and then the ΔNO_x value gradually decreases down to zero after 30 min on stream. This slow process corresponds to the saturation of the Ba sites. The most interesting point is the OCV variations with time. The OCV value corresponds to the potential difference between that of the catalyst-electrode and that of the Au counter-electrode. As reported in the literature [10,17,18], OCV values in a single chamber electrochemical cell refer to the difference in the thermodynamic activity of adsorbed atomic oxygen between the two electrodes. Variations of the potential of the Au counter-electrode prepared from Au paste are negligible in this temperature range [17]. Therefore, recorded variations of OCV are linked to modifications of the oxygen coverage on the catalyst-electrode. Before the introduction of the reactants, sample was only exposed to He and the OCV value was −50 mV at 500 °C, suggesting that the oxygen coverage in presence of traces of oxygen is lower on Pt-Ba/LSCF-GDC than on Au. After the introduction of the NO_x reactant, OCV values rapidly drop to reach a plateau at −160 mV which exactly corresponds to that of ΔNO_x, demonstrating that the catalyst-electrode potential gives a direct evidence of the NO_x storage progress, as already reported on a Pt-Ba electrode [10]. The NO_x storage process strongly decreases the oxygen coverage on the electrode most probably because NO_2 and traces of oxygen are consumed to produce nitrates according to the reaction shown in Equation (1) whereas NO_2 and O_2 can be adsorbed on Au.

$$2NO_2 + \frac{1}{2}O_2 + BaO \rightarrow Ba(NO_3)_2 \quad (1)$$

After the plateau, OCV gradually increases with time, in good concordance with the ΔNO_x decay.

The NO_x SER performance was investigated at 450 °C and 550 °C. Different negative polarizations were applied between the catalytic electrode and the counter electrode (Figures 4 and 5) between −5 V and −7 V. Please note that the ohmic drop was not subtracted from these values. Without any oxygen in the feed, nitrogen oxides, mainly composed of NO, can be electrochemically reduced into N_2 with a 100% selectivity. At 500 °C, NO_x conversions are around 20% and only slightly vary with the negative potential (Figures 4b and 5a) whereas produced negative currents strongly increase (from −2.4 mA to −4.2 mA). This indicates that the generated current is not only produced by the NO_x SER and the N_2 production. One can assume that, under these operating conditions, GDC can be concomitantly electrochemically reduced. On the opposite, at lower temperature, i.e., 450 °C, the NO_x conversion linearly increases with the cathodic potential from 10.5% upon −5 V up to 15.5% upon −7 V. At 450 °C (Figure 4a), current intensities are lower and proportional to the NO_x conversion, suggesting that there is no GDC reduction.

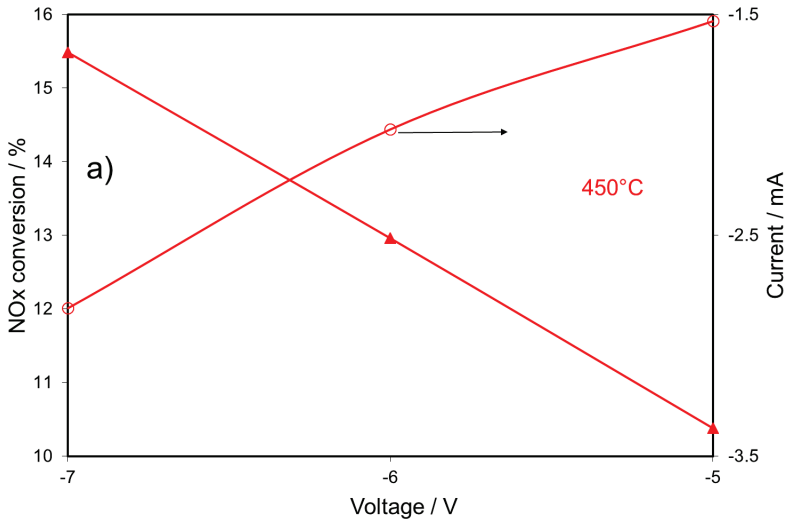

Figure 4. *Cont.*

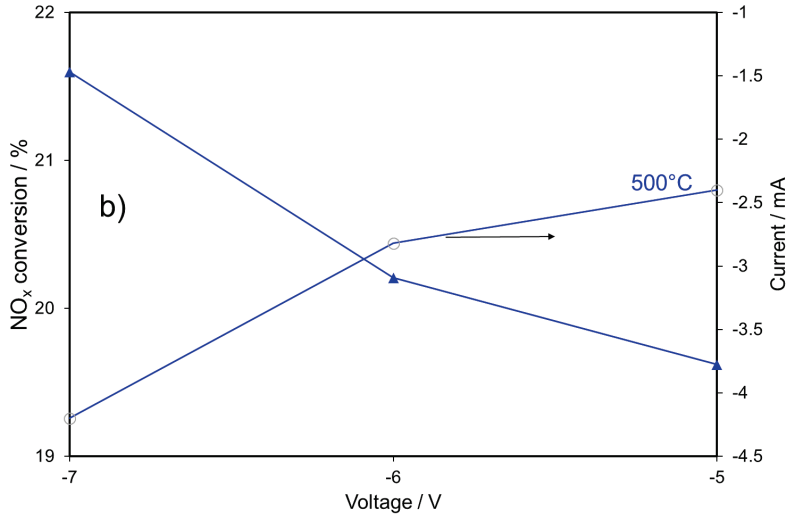

Figure 4. Variations of NO_x conversion and currents as a function of applied potentials (**a**) at 450 °C and (**b**) at 500 °C. Reactive mixture: NO/NO_2: 680 ppm/10 ppm in He.

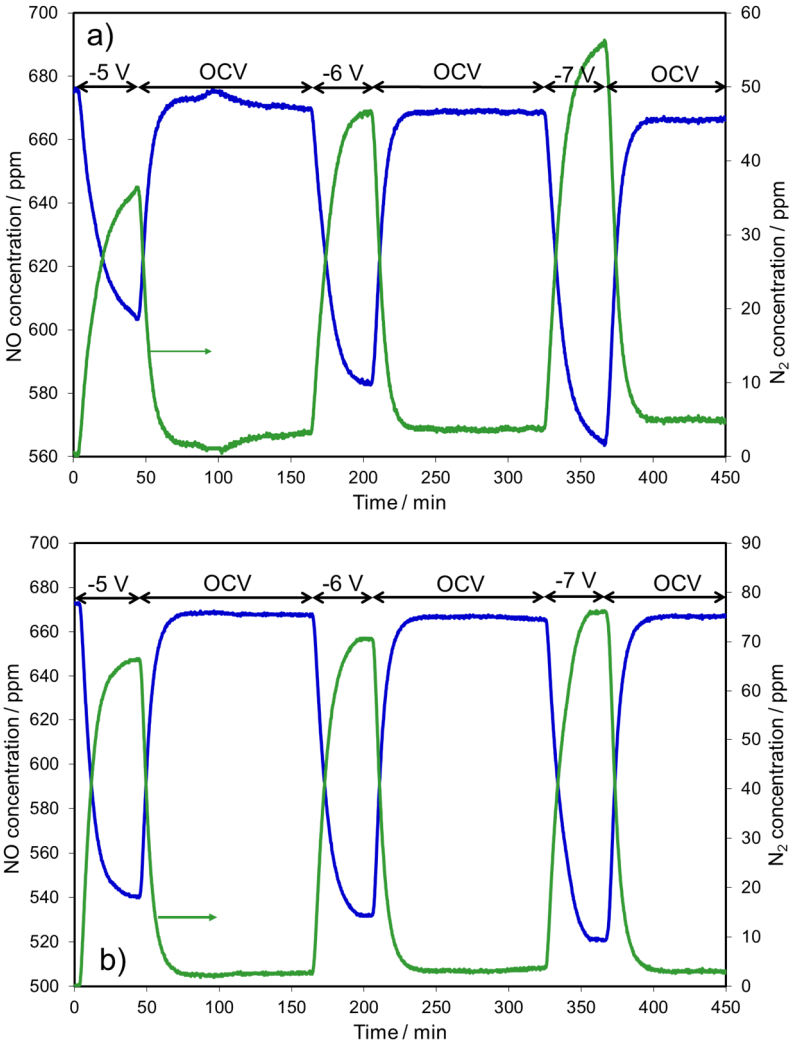

Figure 5. Variations of NO and N_2 concentrations as a function of time at (**a**) 450 °C and (**b**) 500 °C. Reactive mixture: NO/NO_2: 680 ppm/10 ppm in He.

Figure 5 shows that the NO concentration decrease upon cathodic polarizations is gradual and slow. At 450 °C (Figure 5a), the NO concentration does not reach a plateau after more than 40 min polarization. Figure 6 displays variations of the NO concentration and the current with time at 450 °C upon −5 V. The decay of the NO concentration with time is slow, confirming the low kinetic rate of the process. The current variation shows a negative peak after 3 min on stream which corresponds to the ΔNO_x value plateau (Figure 3). This demonstrates that the generated current is dependent on the NO_x storage process and then on the NO_2 production peak.

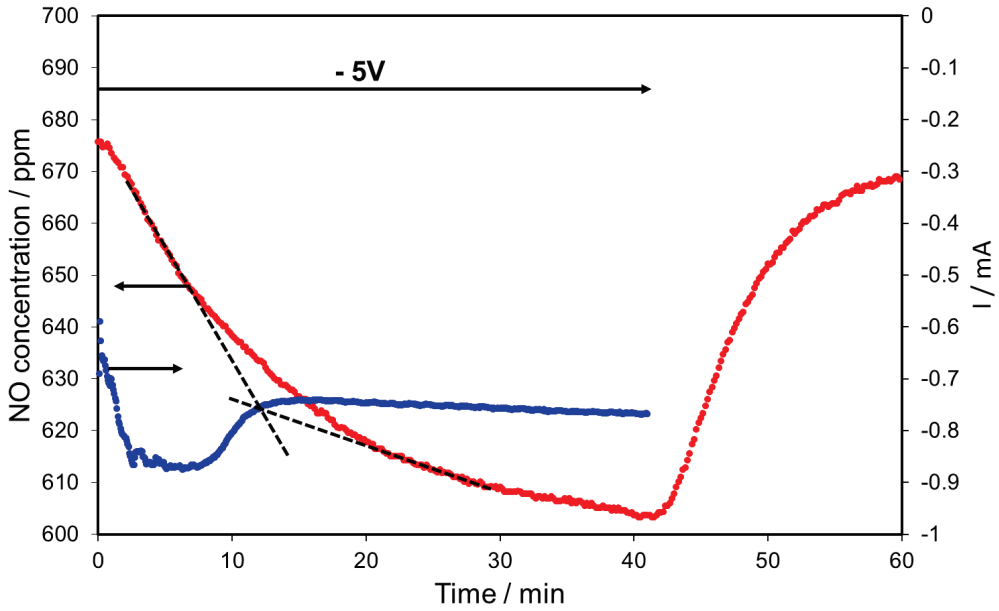

Figure 6. Variations of NO concentration and the current as a function of time at 450 °C. Reactive mixture: NO/NO_2: 680 ppm/10 ppm in He.

2.3. NO_x Electrocatalytic Conversion in the Presence of 1% O_2

Electrocatalytic performances were also investigated in the presence of 1% O_2. At 500 °C, the inlet NO and NO_2 concentrations were about 650 ppm and 40 ppm, respectively, due to the production of NO_2 in the stainless steel pipes. The presence of O_2 concentration increases the steady stable value of NO_2 concentration, as NO is oxidized into NO_2 onto the catalyst-electrode. The NO conversion into NO_2 is around 9% at 500 °C. Values of ΔNO_x are positive right after the reactive mixture introduction (Figure 7). Therefore, as expected, the NO_x storage process is taking place on the catalyst-electrode. Let us note that without any BaO in the electrode, values of ΔNO_x is closed to zero meaning that no NO_x storage is taking place. In presence of BaO, contrary to the experiments without oxygen, ΔNO_x variations do not exhibit a plateau but a sharp peak after 3 min on stream followed by a gradual decay down to −10 ppm. Features of the OCV variations are symmetrically inverted with an initial drop to negative values (−45 mV) followed by a progressive increase up to around 0 mV. The observed slight time shift between the ΔNO_x positive peak and the OCV negative one is only due to the slow response time of the NO_x analyzer. Therefore, these experiments in presence of oxygen confirm that the OCV value is a good sensor of the NO_x storage process. Negative values of OCV indicate that the NO_x storage process is running while a null value points that the catalyst-electrode surface is saturated by nitrates compounds.

Figure 8 gives the variations of NO and NO_2 concentrations upon different voltages from ±3 V to ±1 V at 400 °C. At OCV, the NO conversion into NO_2 is 13%. Whatever the polarization, no production of nitrogen was detected in spite of the NO_x storage process (Figure 7) which proves the presence of Ba. Cathodic and anodic polarizations only induce the electrochemical reduction of NO_2 into

NO and the reverse reaction, respectively. Conversion of NO into NO_2 can reach 15% upon +3 V. The most important point is the ability of the electrode to electrochemically reduce NO_2 into NO for low potentials. At 400 °C, upon −1 V, the NO_2 conversion into NO can reach 30%. However, this conversion is not enhanced by higher cathodic potentials, suggesting that the electrochemical reduction of oxygen becomes predominant. These results are in contradiction with those obtained by Shao et al. [12] with a LSM electrode infiltrated with both BaO and Pt/Al_2O_3. This study has evidenced high conversions of NO_x into N_2 in excess of oxygen upon cathodic potentials. Several causes can explain the different results obtained in this study, such as a quite heterogeneous distribution of the BaO particles in the electrode or a chemical reactivity between BaO and LSCF/GDC materials as proposed by the group of Kammer Hansen [3]. The localization of BaO nanoparticles is quite important since the production of N_2 will depend on the efficiency of the selective electrochemical reduction of $Ba(NO_3)_2$.

$$Ba(NO_3)_2 + 10\,e^- \rightarrow BaO + N_2 + 5\,O^{2-} \quad (2)$$

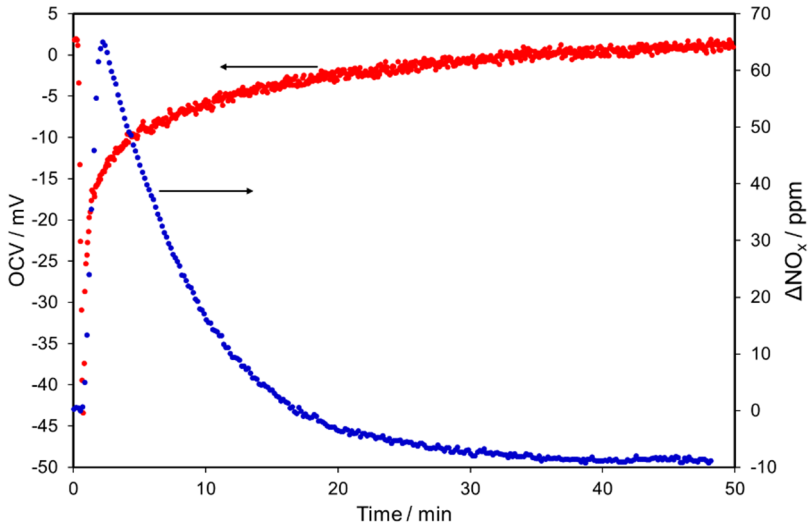

Figure 7. Variations of OCV and ΔNO_x as a function of time at 500 °C. Reactive mixture: $NO/NO_2/O_2$: 650 ppm/40 ppm/1% in He.

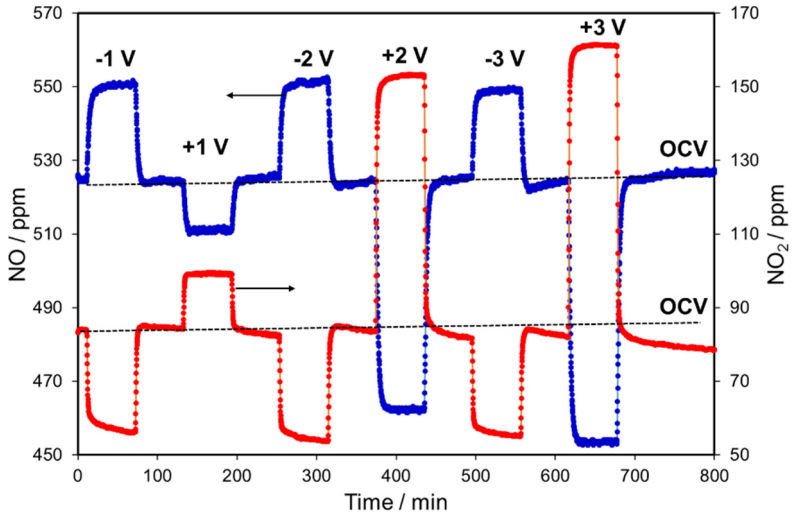

Figure 8. Variations of NO and NO_2 concentrations with time at 400 °C upon polarizations. Reactive mixture: $NO/NO_2/O_2$: 525 ppm/85 ppm/1% in He.

$Ba(NO_3)_2$, located near triple phase boundaries ($gas/O^{2-}/e^-$) in the vicinity of the layer closed to the CGO electrolyte will be much more easily electrochemically reducible than nitrate nanoparticles only present on LSFC grains at the surface of the electrode. During this latter case, the electrochemical reduction of $Ba(NO_3)_2$ will be in strong competition with the oxygen electrochemical reduction. Therefore, if we consider that $Ba(NO_3)_2$ is preferentially formed on LSCF nanoparticles as suggested by the group of K. Kammer Hansen [3], it explains the low kinetic of the reduction process (Figures 5 and 6) observed without oxygen in the feed as nitrates have to diffuse near TPBs (Triple Phase Boundary) and the non-production of N_2 in presence of oxygen as oxygen becomes predominantly electrochemically reduced. Additional characterizations are clearly needed to elucidate the origin of the non-selective electrochemical reduction of NO_x of the ceria-based catalyst electrode.

3. Materials and Methods

3.1. Electrode Preparation

The LSCF (70 wt %)/GDC(30 wt %) composite electrode was prepared by screen-printing (semin-automatic AUREL C890 machine, Modigliana (FC), Italy) [19] on a GDC dense disk (diameter 17 mm, thickness 1 mm) followed by a calcination step at 1200 °C. A gold film was deposited on the opposite side of the GDC pellet in order to act as counter electrode by using a gold paste (Metalor, Oullins, France) annealed at 500 °C for 2 h. Generated micrometric gold particles were found to be inactive for NO_x activation as verified through blank experiments under our experimental conditions. Nanoparticles of Pt and BaO were impregnated in the porosity of the LSCF/GDC electrode. An aqueous solution containing both precursors of $Pt(NH_3)_4(NO_3)_2$ and $Ba(NO_3)_2$ has been prepared. The concentrations of the Pt and Ba solutions were 0.32×10^{-3} mol/L and 1.36×10^{-2} mol/L, respectively. In addition, PVP (polyvinylpyrrolidone) as the surfactant was also added to the solution (10 wt %) to ensure a suitable viscosity. A controlled volume of 40 µL of the Pt/BaO solution has been infiltrated four times successively into the porosity of the LSCF/GDC electrode by using a micropipette. Between each infiltration, the sample was dried for 1 h at 80 °C. The targeted loadings of the Pt and Ba into the porous electrode were 5 $\mu g/cm^2$ and 150 $\mu g/cm^2$, respectively. The sintering temperature of infiltrated electrodes was set at 600 °C for 1 h in air. The Pt nanoparticles in the LSCF/GDC film were characterized by TEM (JEOL 2010 LaB6, JEOL, Peabody, MA, USA) using an extractive replica technique (Figure 2) as described in [20]. A series of composite electrodes without BaO have been also prepared with the same loading of Pt to compare the NO_x storage capacity.

3.2. Measurements of the Electrocatalytic Performances

The Pt-BaO/LSCF-GDC/GDC/Au samples were placed in a single chamber quartz reactor described elsewhere [21]. All the current collectors were made of gold. A gold mesh was placed on the top of the Pt-BaO/LSCF-GDC porous working electrode as current collector. The quartz reactor was installed in a tubular furnace. A potentiostat-galvanostat (Voltalab 80, Radiometer Analytical, Hach Company, Loveland, CO, USA) was used to polarize samples between the catalyst-electrode and the Au counter-electrode.

The reactive mixture gases were composed of NO (4000 ppm in He, LINDE France S.A., Saint-Priest, France, 99.95% purity) and O_2 (LINDE France S.A. 99.95% purity). Helium (LINDE, 99.95% purity) was used as the carrier gas. The gas compositions were adjusted with mass flow controllers (Brooks) with an accuracy of 1%. The testing temperature range was varied from 400 °C to 500 °C. Concentrations of NO, N_2O and NO_2 were monitored by an online analyzer (EMERSON NGA 2000, Emerson Process Management, Bron, France) while N_2 and O_2 contents were determined with a micro-chromatograph (R3000 SRA Instruments, Marcy l'Etoile, France). The NO_x conversion experiments were investigated in presence of 680 ppm NO_x (670 ppm NO and 10 ppm NO_2) without O_2 and for a total flow rate of 42 mL/min. Based on above experiments, the NO_x conversion experiments were also studied in presence of 1% O_2.

The NO_x conversion was calculated as follows:

$$NO_x \text{ conversion} = 100 \times (NO_{x,in} - NO_{x,out})/NO_{x,in} \quad (3)$$

The selectivity to N_2, S_{N_2}, was extracted from the Equation (3).

$$S_{N_2} = 100 \times 2N_{2,out}/NO_{x,in} \quad (4)$$

The production of N_2O was never detected.

4. Conclusions

The NO_x electrochemical catalytic performances of Pt-Ba impregnated LSCF-GDC catalyst-electrode was investigated between 400 °C and 500 °C with and without oxygen in the feed. Pt and BaO nanoparticles were finely dispersed in the catalyst-electrode. Variations of the OCV with time were found to be a good sensor of the NO_x storage process on the electrode. Without oxygen in the feed, NO_x can be selectively electrochemically reduced into N_2, even if the electrochemical process is slow. In presence of O_2, no N_2 production was observed in spite of nitrate formation, showing the key role of Ba nitrate localization in the catalyst-electrode layer. However, the catalyst-electrode was found to be effective at electrochemically reducing NO_2 into NO at 400 °C for low potentials.

Acknowledgments: The authors would like to acknowledge the China scholarship council for the grant of Xi Wang.

Author Contributions: Philippe Vernoux, Yi Xiang, Ning Sheng Cai, Mathilde Rieu and Jean-Paul Viricelle conceived and designed the experiments; Xi Wang, Alexandre Westermann and Mathilde Rieu performed the experiments; Xi Wang, Alexandre Westermann, Philippe Vernoux analyzed the data; Xi Wang and Philippe Vernoux wrote the paper.

Conflicts of Interest: The authors declare no conflict of interest.

References

1. Vestreng, V.; Ntziachristos, L.; Semb, A.; Reis, S.; Isaksen, I.S.A.; Tarrason, L. Evolution of NO_x emissions in Europe with focus on road transport control measures. *Atmos. Chem. Phys.* **2011**, *9*, 1503–1520. [CrossRef]
2. Granger, P.; Parvulescu, V.I. Catalytic NO_x Abatement Systems for Mobile Sources: From Three-Way to Lean Burn after-Treatment Technologies. *Chem. Rev.* **2011**, *111*, 3155–3207. [CrossRef] [PubMed]
3. Werchmeister, R.M.L.; Bentzen, J.J.; Andersen, K.B.; Hansen, K.K. Removal of NO_x with Porous Cell Stacks with $La_{0.85}Sr_{0.15}Co_xMn_{1-x}O_{3+\delta}$-$Ce_{0.9}Gd_{0.1}O_{1.95}$ Electrodes Infiltrated with BaO. *J. Electrochem. Soc.* **2014**, *161*, H663–H669. [CrossRef]
4. Werchmeister, R.M.L.; Hansen, K.K. Electrochemical reduction of oxygen and nitric oxide at low temperature on $Ce_{1-x}Pr_xO_{2-\delta}$ cathodes. *Electrochim. Acta* **2013**, *114*, 474–477. [CrossRef]
5. Huang, T.J.; Wu, C.Y.; Lin, Y.H. Electrochemical Enhancement of Nitric Oxide Removal from Simulated Lean-Burn Engine Exhaust via Solid Oxide Fuel Cells. *Environ. Sci. Technol.* **2011**, *45*, 5683–5688. [CrossRef] [PubMed]
6. Pancharatnam, S.; Huggins, R.A.; Mason, D.M. Catalytic Decomposition of Nitric Oxide on Zirconia by Electrolytic Removal of Oxygen. *J. Electrochem. Soc.* **1975**, *122*, 869–875. [CrossRef]
7. Gür, T.M.; Huggins, R.A. Decomposition of Nitric Oxide on Zirconia in a Solid State Electrochemical Cell. *J. Electrochem. Soc.* **1979**, *126*, 1067–1075. [CrossRef]
8. Hansen, K.K. Electrochemical reduction of O_2 and NO on Ni, Pt and Au. *J. Appl. Electrochem.* **2008**, *38*, 591–595. [CrossRef]
9. Hamamoto, K.; Fujishiro, Y.; Awano, M. Low-Temperature NO_x Decomposition Using an Electrochemical Reactor. *J. Electrochem. Soc.* **2008**, *155*, E109–E111. [CrossRef]
10. Li, X.; Vernoux, P. A new NO_x storage-reduction electrochemical catalyst. *Appl. Catal. B* **2005**, *61*, 267–273. [CrossRef]

11. Shao, J.; Hansen, K.K. Enhancement of NO_x removal performance for $(La_{0.85}Sr_{0.15})_{0.99}MnO_3/Ce_{0.9}Gd_{0.1}O_{1.95}$ electrochemical cells by NO_x storage/reduction adsorption layers. *Electrochim. Acta* **2013**, *90*, 482–491. [CrossRef]
12. Shao, J.; Hansen, K.K. Electrochemical NO_x reduction on an LSM/CGO symmetric cell modified by NO_x adsorbents. *J. Mater. Chem. A* **2013**, *1*, 7137–7146. [CrossRef]
13. Friedberg, A.Z.; Hansen, K.K. Electrochemical reduction of NO with propene in the presence of oxygen on LSCoM/CGO porous cell stacks impregnated with BaO. *J. Solid State Electrochem.* **2015**, *19*, 1611–1620. [CrossRef]
14. Traulsen, M.L.; Andersen, K.B.; Hansen, K.K. NO_x conversion on LSM15-CGO10 cell stacks with BaO impregnation. *J. Mater. Chem.* **2012**, *22*, 11792–11800. [CrossRef]
15. Leng, Y.J.; Chan, S.H.; Jiang, S.P.; Khor, K.A. Low-temperature SOFC with thin film GDC electrolyte prepared in situ by solid-state reaction. *Solid State Ionics* **2004**, *170*, 9–15. [CrossRef]
16. Zha, S.W.; Moore, A.; Abernathy, H.; Liu, M.L. GDC-Based Low-Temperature SOFCs Powered by Hydrocarbon Fuels. *Electrochem. Soc.* **2004**, *151*, A1128–A1133. [CrossRef]
17. Li, X.; Gaillard, F.; Vernoux, P. The Relationship of the Catalytic Activity and the Open-Circuit Potential of Pt Interfaced with YSZ. *Ionics* **2005**, *11*, 103–111. [CrossRef]
18. Hadjar, A.; Hernández, W.Y.; Princivalle, A.; Tardivat, C.; Guizard, C.; Vernoux, P. Electrochemical activation of Pt–Ba/YSZ NO_x TRAP catalyst under lean-burn conditions. *Electrochem. Commun.* **2011**, *13*, 924–927. [CrossRef]
19. Sun, L.P.; Rieu, M.; Viricelle, J.P.; Pijolat, C.; Zhao, H. Fabrication and characterization of anodesupported single chamber solid oxide fuel cell based on $La_{0.6}Sr_{0.4}Co_{0.2}Fe_{0.8}O_{3-\delta}$-$Ce_{0.9}Gd_{0.1}O_{1.95}$ composite cathode. *Int. J. Hydrogen Energy* **2014**, *39*, 1014–1022. [CrossRef]
20. Kambolis, A.; Lizarraga, L.; Tsampas, M.N.; Burel, L.; Rieu, M.; Viricelle, J.P.; Vernoux, P. Electrochemical promotion of catalysis with highly dispersed Pt nanoparticles. *Electrochem. Commun.* **2012**, *19*, 5–8. [CrossRef]
21. Vernoux, P.; Gaillard, F.; Bultel, L.; Siebert, E.; Primet, M. Electrochemical Promotion of Propane and Propene Oxidation on Pt/YSZ. *J. Catal.* **2002**, *205*, 412–421. [CrossRef]